Biological Assessment of Triazine Dendrimer: Toxicological Profiles, Solution Behavior, Biodistribution, Drug Release and Efficacy in a PEGylated, Paclitaxel Construct

Su-Tang Lo,[†] Stephan Stern,[‡] Jeffrey D. Clogston,[‡] Jiwen Zheng,[‡]
Pavan P. Adiseshaiah,[‡] Marina Dobrovolskaia,[‡] Jongdoo Lim,[§] Anil K. Patri,*[‡]
Xiankai Sun,*[†] and Eric E. Simanek*[§]

*Department of Radiology, University of Texas Southwestern Medical Center, Dallas,
Texas 75390, Department of Chemistry, Texas A&M University, College Station,
Texas 77843-3255, and Nanotechnology Characterization Laboratory, Advanced Technology
Program, SAIC-Frederick Inc., NCI-Frederick, Frederick, Maryland 21702*

Abstract: The physicochemical characteristics, *in vitro* properties, and *in vivo* toxicity and efficacy of a third generation triazine dendrimer bearing approximately nine 2 kDa polyethylene glycol chains and twelve ester linked paclitaxel groups are reported. The hydrodynamic diameter of the neutral construct varies slightly with aqueous solvent ranging from 15.6 to 19.4 nm. Mass spectrometry and light scattering suggest radically different molecular weights with the former ~40 kDa mass consistent with expectation, and the latter 400 kDa mass consistent with a decameric structure and the observed hydrodynamic radii. HPLC can be used to assess purity as well as paclitaxel release, which is insignificant in organic solvents or aqueous solutions at neutral and low pH. Paclitaxel release occurs *in vitro* in human, rat, and mouse plasma and is nonlinear, ranging from 7 to 20% cumulative release over a 48 h incubation period. The construct is 2−3 orders of magnitude less toxic than Taxol by weight in human hepatocarcinoma (Hep G2), porcine renal proximal tubule (LLC-PK1), and human colon carcinoma (LS174T) cells, but shows similar cytotoxicity to Abraxane in LS174T cells. Both Taxol and the construct appear to induce caspase 3-dependent apoptosis. The construct shows a low level of endotoxin, is not hemolytic and does not induce platelet aggregation *in vitro*, but does appear to reduce collagen-induced platelet aggregation *in vitro*. Furthermore, the dendrimer formulation slightly activates the complement system *in vitro* due most likely to the presence of trace amounts (<1%) of free paclitaxel. An animal study provided insight into the maximum tolerated dose (MTD) wherein 10, 25, 50, and 100 mg of paclitaxel/kg of construct or Abraxane were administered once per week for three consecutive weeks to non tumor bearing athymic nude mice. The construct showed *in vivo* toxicity comparable to that of Abraxane. Both formulations were found to be nontoxic at the administered doses, and the dendrimer had an acute MTD greater than the highest dose administered. In a prostate tumor model (PC-3-h-luc), efficacy was observed over 70 days with an arrest of tumor growth and lack of luciferase activity observed in the twice treated cohort.

Keywords: Drug delivery; paclitaxel; dendrimer; triazine; melamine; prostate cancer; colon cancer; in vivo; therapy

Introduction

Paclitaxel (PTX) is an antimitotic agent widely used to treat ovarian, breast, lung, head and neck cancers and AIDS-related Kaposi's sarcoma.[1,2] However, due to its poor water solubility, the hydrophobic drug is commonly formulated as Taxol with Cremophor EL (polyoxyethylated castor oil) or other cosolvents before being administered, resulting in dose-limiting toxicity and hypersensitivity in some patients.[3] To overcome this toxicity, other formulations have been explored, most notably, Abraxane, a nanoparticle comprising paclitaxel and serum albumin. Alternatively, incorporation of paclitaxel into polymeric therapeutics is of great interest because the strategy promises to improve the solubility and lower the toxicity of the drug while providing opportunities for targeted-delivery, enhanced biopermeability, and desirable pharmacokinetics.[4−8]

Of the variety of classes of polymers including linear, graft, and star polymers, recent interest has focused on the use of dendrimers to carry and deliver drugs in either noncovalent or covalent manners.[9−11] Notable among these examples are those with tumor uptake and/or efficacy including polylysine and polyesters.[12−15] In most cases, controlled and timely release of the active agent in diseased cells is critical for the drug maximizing efficacy. The study of physicochemical properties of the conjugates will be essential to understand and predict their *in vivo* pharmacokinetic behaviors.

Our interest in triazine dendrimers for use in drug delivery has guided our choice of synthetic targets and methods over the past eight years.[16] Many of the synthetic challenges surrounding this class of molecules have been surmounted as punctuated both by the scale at which these materials can now be produced (up to kilogram)[17] and the sophistication in target structures in terms of orthogonal group[18] or the drugs conjugated including paclitaxel[19,20] and camptothecin.[21] With increased understanding of synthetic methods and scope, preliminary inquiries into biological parameters of interest were made. Cell toxicity appears in polycation dendrimers (24 amines) at 0.1−1 mg/mL in Clone 9,[22,23]

* To whom correspondence should be addressed. E-mail: xiankaisun@utsouthwesternmed.edu; simanek@tamu.edu; patria@mail.nih.gov. E.E.S.: Texas A&M University, Department of Chemistry, MS 3255, College Station, TX 77843-3255; tel, 979-845-4242; fax, 979-845-9452.

† University of Texas Southwestern Medical Center.

‡ NCI-Frederick.

§ Texas A&M University.

(1) Scripture, C. D.; Figg, W. D.; Sparreboom, A. Paclitaxel chemotherapy: from empiricism to a mechanism-based formulation strategy. *Ther. Clin. Risk Manage.* **2005**, *1*, 107–114.

(2) Crown, J.; O'Leary, M.; Ooi, W. S. Docetaxel and paclitaxel in the treatment of breast cancer: a review of clinical experience. *Oncologist* **2004**, *9*, 24–32.

(3) Singla, A. K.; Garg, A.; Aggarwal, D. Paclitaxel and its formulations. *Int. J. Pharm.* **2002**, *235*, 179–192.

(4) Duncan, R. The dawning era of polymer therapeutics. *Nat. Rev. Drug Discovery* **2003**, *2*, 347–360.

(5) Putnam, D. Drug delivery: the heart of the matter. *Nat. Mater.* **2008**, *7*, 836–837.

(6) Aulenta, F.; Hayes, W.; Rannard, S. Dendrimers: a new class of nanoscopic containers and delivery devices. *Eur. Polym. J.* **2003**, *39*, 1741–1771.

(7) Haag, R.; Kratz, F. Polymer therapeutics: Concepts and applications. *Angew. Chem., Int. Ed.* **2006**, *45*, 1198–1215.

(8) Esfand, R.; Tomalia, D. A. Poly(amidoamine) (PAMAM) dendrimers: from biomimicry to drug delivery and biomedical applications. *Drug Discovery Today* **2001**, *6*, 427–436.

(9) Menjoge, A. R.; Kannan, R. M.; Tomalia, D. A. Dendrimer-based drug and imaging conjugates: design considerations for nanomedical applications. *Drug Discovery Today* **2010**, *15*, 171–185.

(10) Boas, U.; Heegaard, P. M. H. Dendrimers in drug research. *Chem. Soc. Rev.* **2004**, *33*, 43–63.

(11) Svenson, S. Dendrimers as versatile platform in drug delivery applications. *Eur. J. Pharm. Biopharm.* **2009**, *71*, 445–462.

(12) Myc, A.; Douce, Thomas B.; Ahuja, N.; Kotlyar, A.; Kukowska-Latallo, J.; Thomas, T. P.; Baker, J. R., Jr. Preclinical antitumor efficacy evaluation of dendrimer-based methotrexate conjugates. *Anti-Cancer Drugs* **2008**, *19*, 143–149.

(13) Fox, M. E.; Guillaudeu, S.; Fréchet, J. M. J.; Jerger, K.; Macaraeg, N.; Szoka, F. C. Synthesis and in vivo antitumor efficacy of PEGylated poly(L-lysine) dendrimer-camptothecin conjugates. *Mol. Pharmaceutics* **2009**, *6*, 1562–1572.

(14) Lee, C. C.; Gillies, E. R.; Fox, M. E.; Guillaudeu, S. J.; Frechet, J. M. J.; Dy, E. E.; Szoka, F. C. A single dose of doxorubicin-functionalized bow-tie dendrimer cures mice bearing C-26 colon carcinomas. *Proc. Natl. Acad. Sci. U.S.A.* **2006**, *103*, 16649–16654.

(15) Kaminskas, L. M.; Kelly, B. D.; McLeod, V. M.; Boyd, B. J.; Krippner, G. Y.; Williams, E. D.; Porter, C. J. Pharmacokinetics and tumor disposition of PEGylated, methotrexate conjugated poly-l-lysine dendrimers. *Mol. Pharmaceutics* **2009**, *6*, 1190–1204.

(16) Simanek, E. E.; Hanan, A.; Lalwani, S.; Lim, J.; Mintzer, M.; Venditto, V. J.; Vittur, B. The eight year thicket of triazine dendrimers: strategies, targets, and applications. *Proc. R. Soc. A* **2010**, *466*, 1445–1468.

(17) Chouai, A.; Simanek, E. E. Kilogram-scale synthesis of a second generation dendrimer based on 1,3,5-triazine using green and industrially compatible methods with a single chromatographic step. *J. Org. Chem.* **2008**, *73*, 2357–2366.

(18) Steffensen, M. B.; Simanek, E. E. Synthesis and manipulation of orthogonally protected dendrimers: Building blocks for library synthesis. *Angew. Chem., Int. Ed.* **2004**, *43*, 5178–5180.

(19) Lim, J.; Simanek, E. E. Synthesis of water-soluble dendrimers based on melamine bearing 16 paclitaxel groups. *Org. Lett.* **2008**, *10*, 201–204.

(20) Lim, J.; Chouai, A.; Lo, S.-T.; Liu, W.; Sun, X.; Simanek, E. E. Design, synthesis, characterization, and biological evaluation of triazine dendrimers bearing paclitaxel using ester and ester/disulfide linkages. *Bioconjugate Chem.* **2009**, *20*, 2154–2161.

(21) Venditto, V. J.; Allred, K.; Allred, C. D.; Simanek, E. E. Intercepting triazine dendrimer synthesis with nucleophilic pharmacophores as a general strategy toward drug delivery vehicles. *Chem. Commun.* **2009**, 5541–5542.

(22) Neerman, M. F.; Zhang, W.; Parrish, A. R.; Simanek, E. E. In vitro and in vivo evaluation of a melamine dendrimer as a vehicle for drug delivery. *Int. J. Pharm.* **2004**, *281*, 129–132.

(23) Chen, H. T.; Neerman, M. F.; Parrish, A. R.; Simanek, E. E. Cytotoxicity, hemolysis, and acute in vivo toxicity of dendrimers based on melamine, candidate vehicles for drug delivery. *J. Am. Chem. Soc.* **2004**, *126*, 10044–10048.
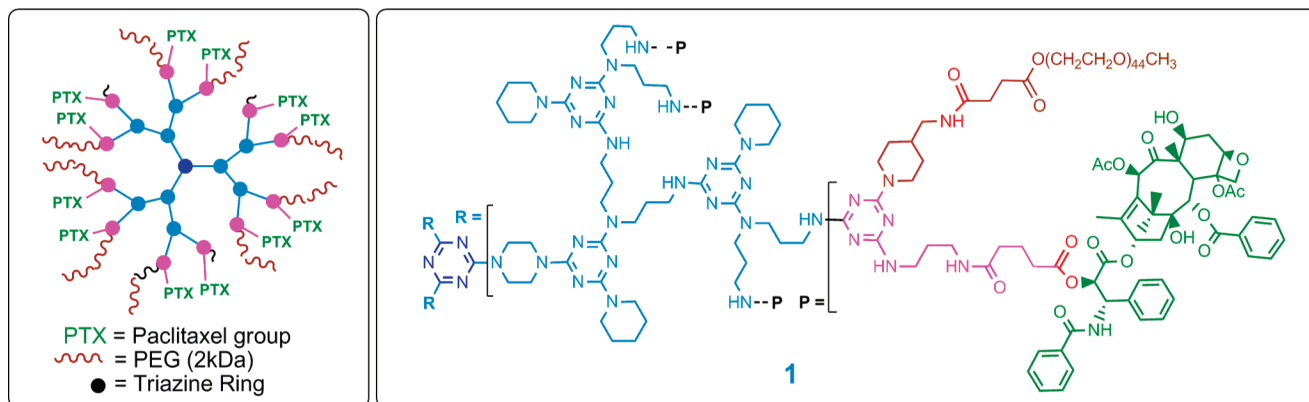
and >1 mg/mL in MCF-7 and A-549 lines.[24] Toxicity is reduced by changing the cationic surface to one that is zwitterionic or neutral as a result of PEGylation.[23] *In vivo*, polycationic (24 amines) triazine dendrimers show no adverse effects as judged by alanine transferase (ALT), an enzyme marker of liver injury, or blood urea nitrogen (BUN), a marker of kidney injury, analysis upon ip injection up to 10 mg/kg.[25] Higher doses in chronic studies showed onset of liver toxicity (ALT and histology) and mortality.[22] PEGylated constructs show markedly lower toxicity with no adverse effects observed at ip doses up to 2.6 g/kg or 1.3 g/kg under iv administration. In addition, we observed that low generation dendrimers show low antigenicity even when charged with antigenic peptides.[24] More recently, a clearer picture of the biodistribution and elimination pathways for these materials has emerged.[20,26] Accordingly, our candidates— second and third generation triazine dendrimers—appear to be promising platforms for nanomedicine. As such, a more complete assessment of biological parameters was warranted. Here, we describe the results of a collaborative effort wherein many biological characteristics of a candidate macromolecular drug, dendrimer **1**, are assessed.

Dendrimer **1** is shown in Chart 1. Three arms radiate from the central core (blue) of dendrimer **1**. The periphery is decorated with 12 paclitaxel groups (green) appended through a 2′-ester linkage (red). Complete drug loading derives from the synthetic methods and purification strategy employed: Twelve paclitaxel-appended dichlorotriazines (pink) are installed on the generation two triazine dendrimer (light blue). Capping with 4-(aminomethyl)piperidine and PEGylation

(brown) installs, on average, 9 PEG chains of 2 kDa each to afford the desired construct, **1**.[20] Accordingly, **1** is 25% weight paclitaxel, 25% weight triazine dendrimer, and 50% weight PEG. Physicochemical and biological assessment of **1** follows.

Experimental Section

Dynamic Light Scattering. Hydrodynamic diameter was measured on a Malvern Zetasizer Nano ZS instrument (Southborough, MA) with back scattering detector (173°, 633 nm laser wavelength) in batch mode at 25 °C using a low volume quartz cuvette (path length 10 mm). Samples were prepared at a concentration of 2 mg/mL in water, 10 mM NaCl, PBS, or saline (154 mM NaCl), and filtered through a 0.2 μm filter (Anotop 10 Plus, Whatman) before a minimum of twelve measurements per sample were made. Hydrodynamic size is reported as the intensity-weighted average over all size populations (Z-avg), and as the intensity weighted and volume-weighted average over a particular range of size populations corresponding to the most prominent peak in the % intensity and % volume distributions (Int-Peak and Vol-Peak), respectively.

Zeta Potential. A Malvern Zetasizer Nano ZS instrument was used to measure zeta potential at 25 °C. Samples were prepared at a concentration of 2 mg/mL in 10 mM NaCl and loaded into prerinsed folded capillary cells for the zeta potential measurements. Sample pH was measured before and after the zeta potential measurements. An applied voltage of 120 V was used. The trace shown in the Supporting Information represents the average of at least three measurements.

HPLC-Based Assessments of Purity. The chromatographic system used to measure sample purity consisted of a degasser (Agilent G1379A, Palo Alto, CA), capillary pump (Agilent G1378A), micro well-plate autosampler (Agilent G1377A), Zorbax 300SB-C8 column (1.0 mm i.d. × 150 mm, 3.5 μm, Agilent), and a diode array detector (Agilent G1315B). The mobile phase consisted of water/acetonitrile (A/B, HPLC grade, 0.14% (w/v) trifluoroacetic acid) at a flow rate of 50 μL/min. The elution gradient was 40% MeCN for 5 min, ramp to 80% MeCN in 80 min, hold at 80% MeCN for 5 min, and ramp down to 40% MeCN in 10 min. The sample volume injected was 5 μL at a concentration of

(24) Neerman, M. F.; Umali, A. P.; Chen, H.-T.; Waghela, S. D.; Parrish, A. R.; Simanek, E. E. Biological evaluation of dendrimers based on melamines. *J. Drug Delivery Sci. Technol.* **2005**, *15*, 31–40.

(25) Zhang, W.; Jiang, J.; Qin, C.; Pérez, L. M.; Parrish, A. R.; Safe, S. H.; Simanek, E. E. Triazine dendrimers for drug delivery: evaluation of solubilization properties, activity in cell culture, and in vivo toxicity of a candidate vehicle. *Supramol. Chem.* **2003**, *15*, 607–616.

(26) Lim, J.; Guo, Y.; Rostollan, C. L.; Stanfield, J.; Hsieh, J.-T.; Sun, X.; Simanek, E. E. The role of the size and number of polyethylene glycol chains in the biodistribution and tumor localization of triazine dendrimers. *Mol. Pharmaceutics* **2008**, *5*, 540–547.

2 mg/mL in HPLC-grade water, and the eluted sample was detected at 227 nm, the absorbance maximum. Samples were run in triplicate.

HPLC-Based Assessment of Paclitaxel Release. Samples of **1** were prepared at 1 mg/mL in water, water at pH 2, acetonitrile, and acetonitrile at pH 2. Over the course of the 3 day experiment, samples were mixed on a rotary shaker placed in an incubator set at 37 °C. An additional sample of **1** (prepared in water) was spiked with 100 μg/mL paclitaxel. The amount of free paclitaxel was determined by RP-HPLC after 3 days. The chromatographic system consisted of a degasser (Agilent G1379A, Palo Alto, CA), capillary pump (Agilent G1378A), micro well-plate autosampler (Agilent G1377A), Zorbax 300SB-C8 column (1.0 mm i.d. × 150 mm, 3.5 μm, Agilent), and a diode array detector (Agilent G1315B). The mobile phase consisted of water/acetonitrile (A/B, HPLC grade, 0.14% (w/v) trifluoroacetic acid) at a flow rate of 50 μL/min. The elution gradient was 40% MeCN for 5 min, ramp to 80% MeCN in 40 min, hold at 80% MeCN for 5 min, and ramp down to 40% MeCN in 10 min. The sample volume injected was 5 μL, and the eluted sample was detected at 210 nm. Samples were run in triplicate.

Molecular Weight Determination by Size-Exclusion Chromatography (SEC) and Asymmetric Flow Field-Flow Fractionation (AFFF) with Multiangle Laser Light Scattering (MALLS) and Refractive Index (RI) Detection. To calculate the value of dn/dc (the change in the refractive index with a change in concentration) needed for the determination of the molecular weight, samples were prepared in PBS at concentrations of 0.1, 0.5, 1, 2, and 3 mg/mL. Briefly, dry sample (typically 30 mg) was added to a preweighed 1.8 mL cryovial, and 1.5 mL of Milli-Q water was added to give a concentration of 20 mg/mL. The solution was then frozen using dry ice and lyophilized overnight. The lyophilized sample was then weighed and the actual sample weight determined. A control (1.8 mL cryovial with 1.5 mL of water) was run in parallel with the sample to correct for any water present in the cryovial. To the known lyophilized sample, an appropriate volume of Milli-Q water was added to give a concentration of 20 mg/mL. Three hundred (300) microliter aliquots (corresponding to 6 mg of sample) were prepared from this stock sample solution, frozen and lyophilized overnight. To the 6 mg sample, 1 mL of PBS was added to give a stock concentration of 6 mg/mL. Samples were prepared at the desired concentrations by diluting the stock solution with PBS. The determination of dn/dc was first performed manually by injecting 1 mL of pure solvent (PBS) into the RI detector (Optilab rEX, Wyatt Technology, Santa Barbara, CA) using a 1 mL disposable syringe. This produces the pure solvent baseline. Next, each sample, starting with the lowest concentration, was manually injected (700 μL) with a new 1 mL disposable syringe. After all the samples were injected, pure PBS was injected again for baseline determination. ASTRA (v5.3.1.5, Wyatt Technology) was used to calculate dn/dc.

The SEC-MALLS apparatus comprised an isocratic pump (Agilent G1310A, Palo Alto, CA), well-plate autosampler

(Agilent G1329A), and TosoHaas TSKgel Guard PW 06762 (7.5 mm i.d. × 7.5 cm, 12 μm) and TSKgel G4000PW 05763 (7.5 mm i.d. × 30 cm, 17 μm, 500 Å) columns (TosoHaas, Montgomeryville, PA). The size exclusion column was connected in-line to a light scattering (MALLS) detector (DAWN EOS, 690 nm laser, Wyatt Technology, Santa Barbara, CA) and a refractive index (RI) detector (Optilab rEX, Wyatt Technology, Santa Barbara, CA). The isocratic mobile phase was PBS (1×, pH 7.5, Sigma D1408, St. Louis, MO) at a flow rate of 1 mL/min. Sample concentration was 3 mg/mL in PBS and filtered through a 0.2 μm filter before 100 μL was injected into the chromatographic system. Dendrimer **1** was analyzed *via* asymmetric flow field-flow fractionation (AFFF) with multiangle laser light scattering (MALLS) and refractive index (RI) for molecular weight determination.

The AFFF-MALLS measurements were performed using instrumentation from Wyatt Technology Corp. (Santa Barbara, CA), which consists of Eclipse2 AFFF controller and DAWN EOS scattering detector and Optilab rEX refractive index detector. The thickness of the AFFF separation channel was defined by a 490 μm PEEK spacer, and a nominal 10 kDa regenerated cellulose membrane served as the flow partition membrane. One hundred (100) microliters of sample was injected into the separation channel and focused against the partitioning membrane for 5 min at a focusing flow rate of 1.0 mL/min. The samples were then separated by a constant cross-flow of 1.0 mL/min during a period of 40 min. The same dn/dc value was used to determine the molecular weight. Two unfiltered samples with concentrations of 3.0 mg/mL and one 0.2 μm-filtered sample with a concentration of 3.0 mg/mL were injected.

Paclitaxel Release in Plasma. In order to determine the concentration of free PTX in **1**, stock solutions of **1** (with concentration of 50, 100, 200, 300, and 400 μg/mL) were prepared in PBS. Aliquots of these stock solutions were analyzed for free PTX using an HPLC assay. In order to determine the rate of release of bound PTX from **1** in plasma, **1** was incubated in plasma (human, rat and mouse) at 37 °C for 48 h. At selected time intervals (0.5, 1, 2, 4, 6, 8, 24, and 48 h), 100 μL aliquots of the plasma samples were collected and prepared for analysis by acetonitrile precipitation. Standard calibration samples were prepared by spiking 100 μL of blank plasma with known paclitaxel concentrations ranging from 0.125 to 25 μg/mL. Plasma samples, 100 μL, were mixed with 0.5 mL of ice-cold acetonitrile that contained 5 μL of 2.5 μg/mL docetaxel as an internal standard. The samples were then centrifuged at 14000 rpm for 20 min to remove precipitated protein. The organic layer was transferred to a clean borosilicate glass tube and evaporated to dryness under a pressured nitrogen gas blowing concentrator (TurboVap LV) at 40 °C. The extraction residue was reconstituted in 1 mL of 20% acetonitrile in water, and 50 μL aliquots were injected into an HPLC system. PTX extraction efficiency in plasma was determined to be between 85−90%. HPLC analysis was performed using a Shimadzu system (LC-20AT pump, SPD-20A UV, a SIL-20AC auto

injector, a C-R3A integrator), and C-18 Zorbax column (5 μm, 4.6 × 150 mm). Note: this is a different HPLC system than was employed earlier.

Chromatographic separations were achieved using a water and acetonitrile gradient elution method (25% acetonitrile from 0 to 5 min, increased linearly to 80% acetonitrile from 5 to 15 min, decreased linearly to 25% acetonitrile from 15 to 17 min), injection volume of 50 μL, UV detection at λ_{max} 227 nm, and a flow rate of 1.0 mL/min. The column temperature was 25 °C, and the column regeneration time between injections was 8 min. The internal standard, docetaxel, and analyte, paclitaxel, elution times were 14.73 and 15.03 min, respectively. Peak area ratio was used to calculate paclitaxel concentrations from the standard calibration curves obtained using tissue matrix standards. A separate calibration in matrix was conducted for each set of tissues analyzed. Data was acquired and processed with LC solution chromatography software from Shimadzu.

Cytotoxicity: Cell lines HepG2, LLC-PK-1, and LS174T. Briefly, **1** and paclitaxel were diluted to 0.000003−300 μM paclitaxel equivalents of **1**, Taxol and Abraxane (for LS174T). Cells were plated in 96-well, microtiter plate format at a density of 50,000 cells per well for HepG2, 25,000 cells per well for LLC-PK1, and 20,000 cells per well for LS174T. Cells were preincubated for 24 h prior to test material addition, reaching an approximate confluence of 80%. Cells were then exposed to test material or media control for 4, 24, 48, and 72 h in the dark, and cytotoxicity was determined using the MTT cell viability and LDH membrane integrity assays. IC_{50} values were approximated from the 48 and 72 h MTT dose−response curves.

LS174T MTT Cytotoxicity Assay-Short Exposure. Using a cell plating density of 20,000 cells per well, cells were plated in 96-well, microtiter plate format. Cells were preincubated for 24 h prior to test material addition, reaching an approximate confluence of 80%. Both **1** and Abraxane were diluted to 0.000005−500 μM paclitaxel equivalent in cell culture media. Cells were then exposed to test material or control media for 1 h, washed with media, and fresh media added. Cytotoxicity was evaluated 6 days later by the MTT cell viability. IC_{50} values were approximated from the MTT dose−response curves.

Caspase Assay. Caspase 3 activity was measured by the Apo-One Homogenous Caspase-3/7 Assay kit (Promega Cat. #TB293, Promega Corp., Madison, WI). Briefly, the test materials were diluted in cell culture media to 0.000003−300 μM paclitaxel equivalents. LS174T cells were plated in 96-well microtiter plate format at 20,000 cells per well in RPMI 1640 cell culture media (2 mM L-glutamine, 10% FBS). The negative control was cell culture media. The positive control was 10 mM acetaminophen. Cells were preincubated for 24 h prior to addition of test sample, reaching an approximate confluence of 80%. Cells were treated with test samples in the dark for 24 and 48 h. Following the treatment period, the test materials were removed. Cells were washed with media, and then incubated for 1 h with kit reagents. Caspase 3 activity was measured using a microtiter plate spectrophotometer at excitation 485 nm and emission 530 nm.

***In Vitro* Immunological Characterization of Sterility.** NCL protocols STE-1.3 (turbidity *Limulus amebocyte* Lysate (LAL)) and STE-2 were followed; complete experimental details can be found on the NCL Web site (http://ncl.cancer. gov/assay_cascade.asp). Compound **1** was tested at 1 mg/ mL concentration.

Hemolysis and Platelet Aggregation. NCL protocols ITA-1 and ITA-2 were followed for this assay; complete experimental details can be found on the NCL Web site (http://ncl.cancer.gov/assay_cascade.asp). Hemolysis was assessed at four concentrations of **1** (1.0, 0.2., 0.04 and 0.008 mg/mL) using Triton-X as the positive control and PBS as the negative control. Three independent samples were prepared for each concentration and analyzed in duplicate (% CV < 25).

Complement Activation. NCL protocol ITA-5 was followed for this assay; complete experimental details can be found on the NCL Web site (http://ncl.cancer.gov/assay_ cascade.asp). Dendrimer **1** was tested at a concentration of 1 mg/mL. Two independent samples were prepared, and each sample was analyzed in duplicate. PBS and cobra venom factor were used as the negative and positive control, respectively.

***In Vivo* Toxicity.** Immediately prior to dosing, both **1** and Abraxane were suspended in PBS. The animal model utilized was 7-week-old female athymic nu/nu mice, three animals per treatment group. The study included four treatment groups (10, 25, 50, and 100 mg paclitaxel/kg) for both **1** and Abraxane, with PBS vehicle control. Treatments were administered by tail vein at 5 mL/kg body weight, once per week for three consecutive weeks. Animals were monitored daily for mortality and signs of pharmacologic or toxicologic effects. Body weights were measured twice weekly and at study termination. Moribund animals (>20% loss in body weight) and animals surviving to planned study termination on day 21 were euthanized by CO_2 asphyxiation, and blood was collected by cardiac puncture for hematological and clinical chemistry analysis. Animals were acclimated to the study environment for two weeks prior to study initiation. Animal rooms were kept at 50% relative humidity, 68−72 °F with 12 h light/dark cycles. Mice were housed by treatment group, with 3 animals/cage (Thoren), with 1/4 in. corncob bedding. Animals were allowed *ad libitum* access to Purina 5L79 rodent chow and RO water. Statistical analyses were conducted using the software program Statistica version 7.1 (StatSoft, Inc., Tulsa, OK). Statistical differences for parametric data were determined by ANOVA, with post hoc comparisons by Dunnet's *t* test or Neuman−Keuls test. Nonparametric data was analyzed by the Kruskal−Wallis ANOVA with multiple comparisons test.

NCI-Frederick is accredited by AAALAC International and follows the Public Health Service Policy for the Care and Use of Laboratory Animals. Animal care was provided in accordance with the procedures outlined in the "Guide

for Care and Use of Laboratory Animals" (National Research Council; 1996; National Academy Press; Washington, DC).

Tissue Culture and Animal Model. The PC-3 cell line was obtained from the American Type Culture Collection (ATCC, Manassas, VA). PC-3 cells or PC-3-h-luc (permanently transfected with luciferase gene) were cultured in T-media at 37 °C in an atmosphere of 5% CO_2 and were passaged at 75% confluence in P150 plates. T-media was supplemented with 5% fetal bovine serum (FBS) and 1× penicillin/streptomycin. Cultured cells were harvested from monolayer using PBS and trypsin/EDTA, and suspended in T-media with 5% FBS. The cell suspension was injected subcutaneously (2×10^6 cells per injection, injection volume 100 μL) into the front flanks (for biodistribution) or the nape of the neck (for treatment) of male SCID (severe combined immunodeficiency) mice with 6−8 weeks of age. After the cell injection, the animals were monitored three times a week by general observations. The tumor was noticed to grow in the first week and allowed to grow three weeks to reach a palpable size for biodistribution or therapeutic efficacy evaluation studies.

Biodistribution Studies in SCID Mice Bearing PC-3 Xenografts. For biodistribution study, 12 mice bearing two tumors (50−500 mg) in the front flanks were randomized into 3 groups ($n = 4$; 4 h, 24 h, and 48 h). Each mouse was intravenously injected with 100 μL of ^{125}I-radiolabeled **1** (~5 μCi/mouse). Mice were sacrificed at 4 h, 24 h, and 48 h postinjection (pi). Organs of interest (blood, heart, lung, fat, liver, spleen, kidney, stomach, intestines, muscle, femur, thyroid, brain, and tumors) were harvested and weighed, and radioactivity was quantified by γ-counter. Standards were prepared, weighed, and counted along with the samples for % ID/g and % ID/organ calculation.

Therapeutic Efficacy Evaluation. PC-3-h-luc tumors were allowed to grow in the nape of the neck for three weeks prior to the first administration of **1**, which was dissolved in Dulbecco's phosphate buffered saline (DPBS) at a concentration of 50 mg of PTX/mL. The tumor-bearing mice were randomized into 5 groups for treatment ($n = 6$): 100 mg/kg PTX equivalents (single dose; 100s); 100 mg/kg PTX equivalents (double doses administered with a 7-day interval; 100d); 200 mg/kg PTX equivalents (single dose; 200s); 200 mg/kg PTX equivalents (double doses administered with a 7-day interval; 200d); and a PBS control. The administration was through the tail vein. Tumor size in mm³ was estimated using the formula $(\pi/6)W^2L$, where L is the longest diameter of the tumor and W is the width perpendicular to the longest diameter. The tumor size was measured every other day, and the tumor cell viability was monitored by a bioluminescence imaging system (BLI) weekly. To minimize the individual animal difference, the tumor volume ratio (tumor size change in a mouse) at a given day was referenced to the tumor size of the same mouse at day 4, which was normalized to 1 for all animals. Statistical analysis was performed by using Prism statistic program (GraphPad, San Diego, CA). Body weights were monitored throughout.

Bioluminescent Imaging (BLI). *In vivo* BLI was used to noninvasively monitor the tumor cell viability in mice bearing PC-3-h-luc tumor. Prior to imaging, mice were anesthetized by inhaling an isoflurane−oxygen mixture (3% isoflurane, 3% oxygen) and then injected intradermally with 80 μL of 40 mg/mL of D-luciferin (Gold Biotechnology Inc., St. Louis, MO) in PBS. An IVIS cooled charge coupled device (CCD) camera apparatus (Xenogen Corp., Alameda, CA) was used for capturing photon emissions from the tumors with an acquisition time between 5 sec to 2 min depending on the photon intensity. The Living Image software package from Xenogen was used for imaging data analysis in the regions of interest (ROI), and the maximum values were obtained in photon/second/cm²/steradian. The Prism statistic program (GraphPad, San Diego, CA) was used for statistic data analysis.

Results and Discussion

Solution Phase Behavior: Monomeric Species or Micellar Aggregate? Our mental image of what **1** looks like in solution is dependent on solvent. In the extreme, two solvents are of importance, simple aqueous solutions and the physiologic milieu. In simple aqueous solvents, we hypothesize that **1** exists primarily as an aggregate, perhaps a decamer. Using dynamic light scattering, no significant difference in diameter was observed for **1** dispersed in 10 mM NaCl (18.5 nm), PBS (19.4 nm), or saline (18.9 nm). In water, the size was notably reduced by 4 to 15.6 nm. Larger aggregates approaching micrometer scale were also recorded.

Corroborating the formation of aggregates is data derived from size exclusion chromatography using multiple angle laser light scattering (SEC-MALLS). By MALDI-TOF, the expected mass of approximately 40 kDa is observed for **1**. The light scattering signal from SEC-MALLS shows two peaks, the main peak eluting at ~8.5 min and a smaller peak at ~6.5 min. Based on the refractive index signal, the first peak is present in very low amounts and elutes with the solvent peak. This behavior implies that it is larger than the size limit of the column (1500 kDa) and may therefore represent aggregates of **1** with the previously suggested submicrometer-scale size. The main peak has a molecular weight of 400 kDa, leading to the hypothesis that in solution **1** assembles into a structure with approximately 10 units. Additional corroboration for this aggregation tendency exists: These values agree with the molecular weight estimate obtained through AFFF-MALLS.

Asymmetric field flow fractionation (AFFF) provides separation of a sample in an AFFF channel by applying a cross-flow to press the sample against the partition membrane. In such a setup, small molecules elute first, followed by larger molecules. The molecular weights of two duplicate samples of unfiltered **1** were determined to be 420.2 kDa and 425.1 kDa, respectively. A lower molecular weight estimate of 373.5 kDa is obtained by filtering the sample. This behavior is consistent with the hypothesis that filtration removes some of the higher molecular weight aggregates.
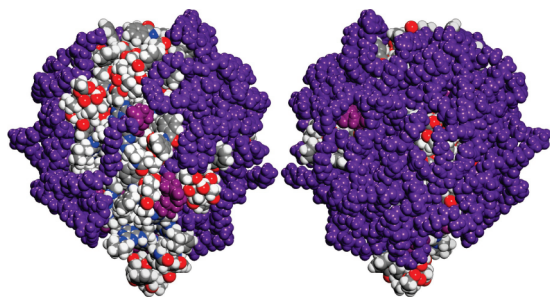
Figure 1. Gas phase simulations of **1** with nine PEG chains reveal opportunities for hydrophobic patch formation on one face derived largely from paclitaxel groups. Each PEG chain is colored violet with purple used to indicate the site of attachment to the dendrimer. Dendrimer and paclitaxel are indicated using conventional colors (C = gray, H = white, N = blue, O = red). Little of the triazine dendrimer is apparent.

The existence of aggregates is not inconsistent with previous observations. The hydrogen bond donor−acceptor capabilities of these triazines has led to the observation of gelation of organic solvents at low concentrations.[27] Similar sized triazine dendrimers bearing approximately 10 PEG chains showed anomalously high elimination half-lives compared with other dendrimers.[26] Surprisingly, however, **1** does not behave similarly *in vivo*. It appears that the installation of paclitaxel groups (or other, much lesser perturbations in structure) leads to biodistribution profiles that match other hypothetically monomeric species in clearance rate, but the accumulation apparent in the liver is consistent with either aggregates or active uptake.[20]

The molecular basis for aggregation likely derives in part from the Janus nature of these molecules. Computation in the gas phase reinforces a picture wherein the hydrophobic core of the triazine dendrimer and paclitaxel groups collapse and orient PEG chains in a common direction (Figure 1). This provides for the exposure of a hydrophobic patch that could cause aggregation. The zeta potential for **1** was measured in 10 mM NaCl and was -1.8 ± 0.7 mV ($n = 3$) at pH 8.4. Zeta potential provides a measure of the electrostatic potential at the surface of the interaction of the electrical double layer surrounding a particle and the bulk medium, which is related to the particle's surface charge. The zeta potential distribution recorded is consistent with a PEGylated nanoparticle of unspecified dimensions.

Assessing Purity and Paclitaxel Release. The purity of **1** was determined by RP-HPLC, and the resulting chromatogram shows two distinct features (Figure 2). The first feature is identified as paclitaxel based on comparison in retention times to free paclitaxel injected alone. This peak integrates for approximately 0.8% of the area leading to the claim that **1** contains less than 1% free paclitaxel. The second feature has an elution profile that allows for the main dendrimer
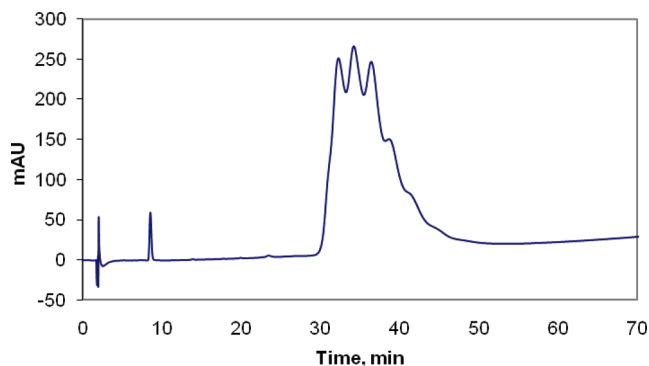
Figure 2. Chromatogram of **1** showing free paclitaxel (∼9 min) and a series of peaks (attributed to differing degrees of PEGylation) corresponding to dendrimer **1**.

peak to be resolved (though not baseline) into at least 6 peaks. These peaks may represent dendrimers with different loadings of paclitaxel or different loadings of PEG. We favor the latter explanation based on our evaluation of the chemistry and the belief that an average of 9 PEG chains of the possible 12 is present on the dendrimer. Unfortunately to date, we have been unable to obtain MALDI-TOF for the fractionated peak: such efforts may ultimately be required should we arrive at competitive efficacy at the clinically relevant doses. It might be that these peaks represent different aggregation states of **1**, but both the clear resolution of species and the high organic content of the solvent lead us to favor incomplete PEGylation. Similar resolution of mixtures has been reported by Banasek Holl and co-workers who investigate the substoichiometric derivatization of PAMAM dendrimers with methotrexate and folate.[28]

The resolution of free paclitaxel and dendrimer offers a facile mechanism to assess paclitaxel release under a variety of conditions including the presence of plasma derived from humans, rats, and mice. Solvolysis of the 2′-ester was probed by incubating **1** at 37 °C in water and acetonitrile at both neutral pH and pH 2. These samples were compared with an aqueous solution of **1** stored at 4 °C. The traces show no release of paclitaxel under the conditions probed. To establish that solubility limitations of paclitaxel did not lead to this conclusion as a result of artifact, a sample of **1** spiked with a known amount of paclitaxel was run. The data suggest that aqueous formulations of **1** may have reasonable stability. These observations lessen significantly our concerns about the effect that dialysis has on premature drug release.

However, very different results were observed in the presence of plasma. Such studies are the result of careful calibration and control, because unlike the plasma-free studies, sample aliquots are not directly injected into the HPLC. Instead, an extraction protocol is followed with validity documented by establishing extraction efficiency of paclitaxel from plasma. Docetaxel was used as an internal

(27) Zhang, W.; Gonzalez, S. O.; Simanek, E. E. Structure-activity relationships in dendrimers based on triazines: Gelation depends on choice of linking and surface groups. *Macromolecules* **2002**, *35*, 9015–9021.

(28) Mullen, D. G.; Fang, M.; Desai, A.; Baker, J. R., Jr.; Orr, B. G.; Holl, M. B. B. A Quantitative Assessment of Nanoparticle-Ligand Distributions: Implications for Targeted Drug and Imaging Delivery in Dendrimer Conjugates. *ACS Nano* **2010**, *4*, 657–670.
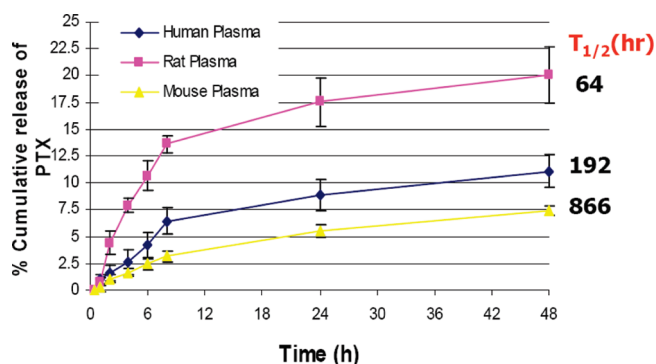
Table 1. Cumulative Release of Paclitaxel from Serums Derived from Human, Rat, and Mouse Sources

time (h)	% cumulative release ± SD		
	human plasma	rat plasma	mouse plasma
0.5	0.07 ± 0	0.07 ± 0	0.07 ± 0
1.0	0.94 ± 0.57	0.76 ± 0.33	0.27 ± 0.35
2.0	1.6 ± 0.73	4.38 ± 1.10	1.04 ± 0.34
4.0	2.63 ± 1.19	7.90 ± 0.61	1.64 ± 0.33
6.0	4.19 ± 1.11	10.65 ± 1.41	2.40 ± 0.45
8.0	6.41 ± 1.24	13.61 ± 0.76	3.14 ± 0.48
24	8.84 ± 1.49	17.56 ± 2.24	5.50 ± 0.53
48	11.08 ± 1.50	20.06 ± 2.66	7.43 ± 0.48

Table 2. Cytotoxicity Data for Three Different Cell Lines

compd	Hep G2 (μM)		LLC-PK1 (μM)		LS174T (μM)	
	48 h	72 h	48 h	72 h	48 h	72 h
dendrimer **1**	>300	3	5	1	0.1	0.1
Taxol	10	0.03	0.005	0.001	0.0003	0.0001
Abraxane	na	na	na	na	0.1	0.1

standard as both compounds are very similar in structure and gave sharp peaks with baseline resolution. No endogenous or extraneous peaks were observed interfering with the separation and quantitation. Paclitaxel was stable during the time of analysis, and no degradation products were found using the acetonitrile/water mobile phase system. The calibration curves for paclitaxel in plasma matrix were linear in the range of 0.5−2.5 μg/mL. Correlation coefficients, $r = > 0.99$ were found for paclitaxel/docetaxel peak areas versus theoretical paclitaxel concentrations in plasma standards. The limit of detection (LOD) was established to be 0.125 μg/mL using a 100 μL plasma sample. At higher concentrations, 90% extraction efficiency is obtained.

While our long-term interest focuses on human chemotherapy, our reliance on mouse and other models of disease led us to examine release of paclitaxel from **1** in the serums derived from mice, rats, and humans. Table 1 shows the cumulative release of paclitaxel from these three serums over a 48 h period. Clearly, release appears species dependent and slow. Indeed, half-lives estimated from the data were calculated to be 64 h, 192 h, and 886 h for rat serum, human serum, and mouse serum, respectively. The data of Table 1 are plotted in Figure 3. These parameters open up a wide space for dosing options in future efficacy studies.

Biological Activity *in Vitro*. In route to determining a therapeutically useful dosing strategy for **1**, cytotoxicity against a panel of cell lines, caspase 3 activation, and hemolytic potential were probed *in vitro*. Taxol and Abraxane formulations serve as a useful comparison.

Figure 3. Cumulative release (in %) of paclitaxel from **1** in human, rat, and mouse plasma.

Cytotoxicity. Cytotoxicity was probed in human hepatocarcinoma (Hep G2) cells, porcine renal epithelial (LLC-PK1) cells, and human colon carcinoma (LS174T) cells (subsequently used in xenografts). The maximum concentrations tested in these studies were 300 μM paclitaxel equivalents of **1**, Taxol, and Abraxane. Treatment of cells with both materials resulted in a dose- and time-responsive loss of cell viability as measured by the MTT assay and loss of membrane integrity as measured by the LDH leakage assay. The LDH values did not correlate with the MTT data at high concentrations and later time points, at which point LDH inhibition/degradation appeared to occur. The data for these experiments are shown in Table 2. Across all cell lines, **1** showed markedly lower toxicity than Taxol. Abraxane was used in addition for LS174T, as this line was chosen for the xenograft model.

Both **1** and Taxol treated cells demonstrated similar morphology at the 24 h time point and high concentration with changes characteristic of apoptosis, including rounding of cells and loss of cell adhesion (See Supporting Information for micrographs). As earlier, the LDH values did not correlate with the MTT data at high concentration and later time points, at which point LDH inhibition/degradation appeared to occur. The dose−response curve for Taxol displayed two horizontal asymptotes, with an intervening plateau, and at the highest concentrations complete loss of cell viability. By contrast, both **1** and Abraxane formulations only displayed one asymptote, with an extended plateau at high concentrations that did not reach 0% of control viability.

A short exposure analysis was performed wherein the MTT assay was used to evaluate cytotoxicity in LLC-PK1 cells under the assumption that a short exposure/long incubation regimen may be more relevant to *in vivo* exposures. The approximated IC_{50} values were 10 μM for **1**, and 1 μM for Abraxane. The dose−response curve for both **1** and Abraxane displayed near complete loss of cell viability at the highest concentrations.

Caspase 3/7 Activation. The observed apoptotic phenotype prompted us to confirm this observation using a caspase 3 apoptosis assay in LS174T cells. Treatment of the LS174T cells with **1** and Taxol resulted in a significant dose responsive increase in caspase 3/7 activity over control at 24 and 48 h as indicated by the caspase 3/7-dependent cleavage assay (Supporting Information). The increase in caspase 3 activity mimicked the cytotoxicity profile of each agent, and was greater for Taxol than for **1**, leading us to conclude that the cytotoxicity in LS174T cells involves caspase 3/7 dependent apoptosis, as has been described in the literature for paclitaxel cytotoxicity.[29]

***Table 3.*** Hematology and Clinical Chemistry of **1**[a]

	vehicle control (PBS)	prodrug **1** dose (mg PTX/kg body weight)			
		10	25	50	100
White Blood Cells ($10^3/\mu$L)					
no. of animals	3	2	2	2	3
total leukocytes	8.86 ± 3.82	9.13 ± 1.09	9.34 ± 2.74	7.35 ± 4.79	8.75 ± 3.00
neutrophils	2.01 ± 0.67	2.30 ± 0.21	2.95 ± 0.72	2.09 ± 0.98	2.20 ± 0.91
lymphocytes	6.41 ± 2.98	6.29 ± 0.83	5.94 ± 1.92	4.57 ± 3.75	6.14 ± 2.02
macrophage/monocytes	0.41 ± 0.15	0.52 ± 0.04	0.40 ± 0.08	0.50 ± 0.22	0.28 ± 0.15
eosinophils	0.020 ± 0.026	0.025 ± 0.007	0.040 ± 0.014	0.13 ± 0.11	0.09 ± 0.06
basophils	0.007 ± 0.006	0.010 ± 0.00	0.0100 ± 0.0001	0.06 ± 0.07	0.037 ± 0.012
Clotting Potential					
platelet count (10^3/mL)	811 ± 66	750 ± 43	664 ± 90	564 ± 73[a]	578 ± 54[a]
mean platelet vol (fL)	5.1 ± 0.2	5.1 ± 0.2	5.2 ± 0.1	5.3 ± 0.2	4.9 ± 0.2
Red Blood Cells					
no. of animals	3	2	2	2	2
total erythrocyte count (M/μL)	9.35 ± 0.41	9.53 ± 0.14	8.63 ± 0.37	8.78 ± 0.74	8.63 ± 1.62
hemoglobin (hb) concn (g/dL)	14.8 ± 0.5	15.1 ± 0.1	13.9 ± 0.1	13.8 ± 1.8	14.3 ± 1.7
hematocrit (%)	51.6 ± 0.7	51.8 ± 1.4	46.9 ± 0.1	49.8 ± 6.0	48.9 ± 8.9
mean corp vol (fL)	54.9 ± 3.6	54.8 ± 0.1	54.3 ± 2.3	56.6 ± 2.1	56.7 ± 0.4
mean corp hb (Pg)	15.8 ± 0.9	15.8 ± 0.1	16.1 ± 0.8	15.7 ± 0.8	16.7 ± 1.4
mean corp hb concn (g/dL)	28.6 ± 0.8	29.1 ± 0.6	29. Six ±0.2	27.8 ± 0.4	29.5 ± 2.2
red cell distr width (%)	17.2 ± 1.2	16.5 ± 1.1	16.4 ± 0.4	15.6 ± 0.2	16.0 ± 0.4
Electrolyte Balance (mmol/L)					
no. of animals	3	3	3	3	3
calcium	10.1 ± 0.1	9.9 ± 0.1	9.8 ± 0.2	9.8 ± 0.3	9.7 ± 0.1
phosphate	8.2 ± 0.9	7.3 ± 1.0	8.0 ± 0.6	8.3 ± 1.0	9.1 ± 0.2
potassium	7.6 ± 0.5	7.3 ± 0.2	7.3 ± 0.2	17.6 ± 17.2	7.4 ± 0.2
sodium	155 ± 24	154 ± 3	155 ± 3	157 ± 1	154 ± 2
Carbohydrate Metabolism					
glucose (mmol/L)	172 ± 24	177 ± 15	166 ± 16	150 ± 14	159 ± 10
Pancreatic Function					
amylase (U/L)	963 ± 81	182 ± 108	928 ± 63	807 ± 171	893 ± 110
Liver Function: Hepatobiliary					
total bilirubin (mg/dL)	0.4 ± 0.1	0.4 ± 0.0	0.3 ± 0.1	0.3 ± 0.0	0.4 ± 0.1
Liver Function: Hepatocellular					
alanine aminotransferase (U/L)	79 ± 16	86 ± 5	74 ± 20	82 ± 10 y>	81 ± 5
Kidney Function					
creatinine (mmol/L)	0.2 ± 0.0	0.2 ± 0.0	0.2 ± 0.0	0.2 ± 0.0	0.2 ± 0.0
urea nitrogen (mg/dL)	19 ± 1	19 ± 4	20 ± 4	24 ± 6	21 ± 3
Others					
albumin (g/L)	4.1 ± 0.1	3.7 ± 0.3	3.9 ± 0.3	4.1 ± 0.1	3.0 ± 0.1
alkaline phosphatase (U/L)	79 ± 16	86 ± 5	74 ± 20	82 ± 10	81 ± 5
globulin (calcd, g/L)	1.4 ± 0.1	1.4 ± 0.3	1.4 ± 0.4	1.2 ± 0.3	1.1 ± 0.3
A/G ratio	3.0 ± 0.2	2.8 ± 0.8	2.9 ± 0.8	3.7 ± 0.9	3.6 ± 0.8
total protein (g/L)	5.5 ± 0.2	5.1 ± 0.2	5.3 ± 0.3	5.3 ± 0.2	5.1 ± 0.3

[a] Deviation of platelet count is currently attributed to sample preparation.

Sterility. Samples of **1** derive ultimately from ultrafiltration and/or dialysis. To probe for potential contamination with bacterial lipopolysaccharide and cell forms of bacteria, yeast and mold, NCL protocols STE-1.3 (turbidity *Limulus amebocyte* lysate (LAL)) and STE-2 were followed (see http://ncl.cancer.gov/assay_cascade.asp for complete experimental details) using **1** at 1 mg/mL. No bacterial, yeast or mold contamination was detected. Endotoxin levels, as estimated by kinetic turbidity LAL assay, were 1.13 endotoxin units (EU)/mg. Clinically, this level of endotoxin is acceptable for a maximum dose of **1** that does not exceed 4.4 mg/kg/h.

Platelet and Red Blood Cell Effects and Complement. In addition to cytotoxicity and contamination, dosing could be limited by both hemolysis and platelet interactions. In short, **1** does not affect the integrity of red blood cells, showing no hemolytic potential over four concentrations: 1 mg/mL,
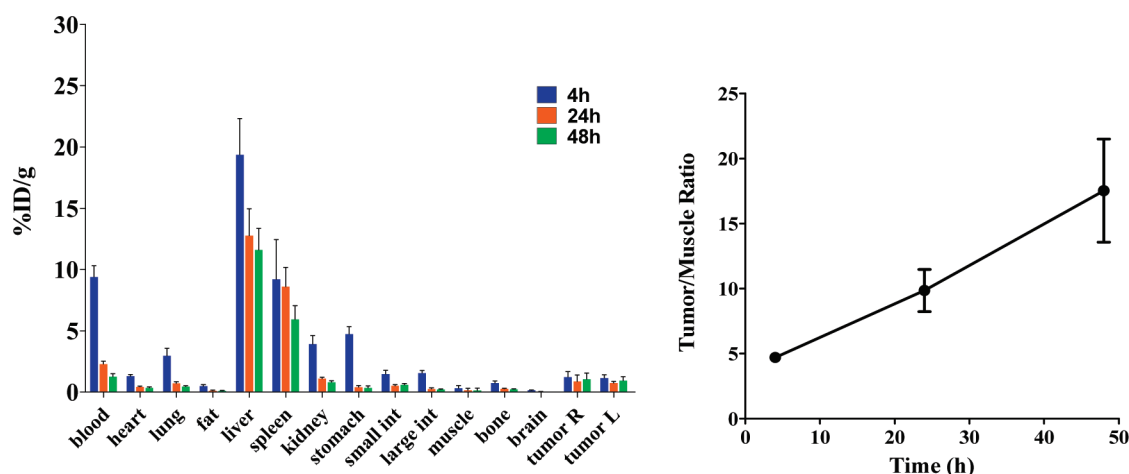
Figure 4. Biodistribution and tumor localization of **1** in SCID mice bearing PC-3 xenografts showing tumor/muscle ratios at different time points, respectively.

0.2 mg/mL, 0.04 mg/mL and 0.008 mg/mL. To evaluate nanoparticle effects on human platelets *in vitro*, **1** was tested over an identical concentration range. While no platelet aggregation was observed (percent aggregation was always below the 20% assay threshold), interestingly, **1** did inhibit collagen-induced platelet aggregation *in vitro* (percent aggregation below 20%). These effects appeared to be independent of particle concentration over the range tested.

Separately, complement activation was examined at 1 mg/mL of **1**. Paclitaxel is known to be immunoreactive with literature reports of hypersensitivity reactions and complement activation by paclitaxel in chremophor formulations. Given the trace amounts (<1% free paclitaxel), we expected that it was likely that the complement activation would occur. Activation did occur. While previous studies with PAMAM dendrimers have shown no complement activation irrespective of dendrimer size (generation) or surface charge, we cannot extrapolate this result to the triazine architectures at the present time. The very slight induction observed does not give us cause for concern at this time.

Biological Activity *in Vivo*. Since their inception, triazine dendrimers have evoked concerns about biocompatibility. To this end, a thorough analysis of blood chemistries was performed over a hypothetical dosing regime based on the Abraxane dosing schedule. Briefly, the repeat-dose regimen in the athymic nude (nu/nu) mouse model was performed at doses of 10, 25, 50, and 100 mg paclitaxel/kg of **1** (or Abraxane) administered once per week for three consecutive weeks to non tumor bearing athymic nude mice. Study end points included daily clinical observation, biweekly body weight measurement, hematology and clinical chemistry. Over the course of these studies, there were no deaths nor any abnormal clinical observations, noted for any of the animals treated with either **1** or Abraxane. The weights of

**Table 4.** Cumulative Excretion Data of **1** Found in the Urine and Feces

% ID	24 h	48 h	72 h
urine	26.6	31.5	34.8
feces	1.6	2.1	2.5

animals in receiving **1**, Abraxane or PBS were observed to decrease slightly following dosing, and recover several days later. There were no significant differences in body weight between the treatment and control groups. Decreases in body weight gain did not follow a dose-dependent trend for either the **1** or Abraxane groups. The hematology parameters for **1** are summarized in Table 3. There was a sporadic finding of statistically significant decreases in mean platelet count for **1** (and Abraxane groups) that was not dose dependent—an observation which is currently attributed to sample preparation. No statistically significant differences in the remaining hematology parameters were identified. A similar panel of clinical chemistries executed is also shown with no significant differences noted. No maximum tolerated dose was defined.

Biodistribution. A biodistribution study of **1** was recently concluded (Figure 4) and is included here for completeness, as this data and the synthesis—uniquely—were previously reported.[20] The distribution half-life ($t_{1/2\alpha}$) and elimination half-life ($t_{1/2\beta}$) were 0.4 and 15.3 h, respectively. Tumor uptake was observed, but was modest. While the tumor:blood ratio was significantly lower than desirable (0.8 at 48 h), the tumor:muscle ratio was found to be 14.6 at 48 h. Biodistribution of dendrimers is impacted by size with small dendrimers excreted through the kidneys and larger dendrimers accumulating in the liver.[30] The accumulation of dendrimer **1** in the liver and spleen presumably due to the sequestration by the reticuloendothelial system (RES) is consistent with the hypothesis of aggregation *in vivo*.

(29) Weigel, T. L.; Lotze, M. T.; Kim, P. K.; Amoscato, A. A.; Luketich, J. D.; Odoux, C. Paclitaxel-induced apoptosis in non-small cell lung cancer cell lines is associated with increased caspase-3 activity. *J. Thorac. Cardiovasc. Surg.* **2000**, *119*, 795–803.

(30) (a) Tomalia, D. A.; Reyna, L. A.; Svenson, S. Dendrimers as multipurpose nanodevices for oncology drug delivery and diagnostic imaging. *Biochem. Soc. Trans.* **2007**, *35*, 61–67, 2007. (b) Kobayashi, H.; Brechbiel, M. W. *Mol. Imaging* **2003**, *2*, 1–10.
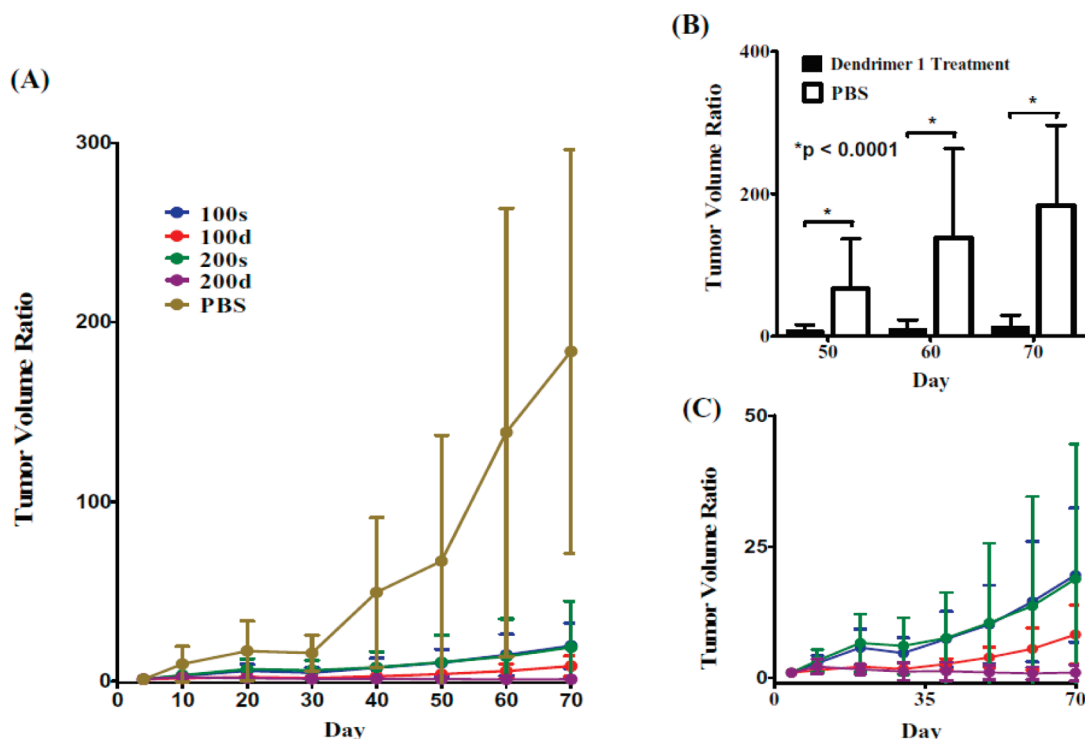
Figure 5. Therapeutic efficacy of **1** in SCID mice bearing PC-3-h-luc xenografts. (A) Tumor volume changes measured by caliper during the 10-week treatment period (tumor volume ratio = tumor size at a given time/tumor size at day 4 post treatment). (B) Statistical comparison between the treatment groups (pooled data from 100s, 100d, 200s, and 200d shown as black columns) and the PBS control. Significant therapeutic efficacy ($p < 0.0001$) was seen starting from day 50 post treatment. (C) Expanded portion of the treatment group data in (A). The abbreviations reflect the amount of paclitaxel in mg of PTX/kg (100 or 200) and whether a single (s) or double (d) administration was used.

Satisfyingly, the majority of **1** was excreted through urine (~30% ID), while less than 3% ID was found in the feces (Table 4).

The antitumor activity of **1** (at 15 and 30 mg PTX/kg) and Abraxane (at 5 and 10 mg/kg) was initially assessed in an LS174T colon cancer xenograft in direct comparison to Abraxane. Doses were administered by tail vein injection once daily for five consecutive days (qd × 5) based on an earlier report.[31] Unfortunately, no dose responsive inhibition of tumor growth was observed for **1**, and no statistically significant difference in tumor volume was obtained for all treatment groups ($P = 0.8$) on day 20. There were no significant clinical abnormalities (body weight or organ weight on necropsy) nor treatment-related mortality observed in any of the treatment groups (data not shown).

However, in a prostate cancer model (PC-3-h-luc) at higher doses, therapeutic efficacy of **1** was observed (Figure 5). Mice were inoculated with 2×10^6 PC-3-h-luc cells in the nape of the neck. When the tumors reached the size range

of 0.4–250 mm^3 (3 weeks after inoculation), the animals were randomized into five groups for the treatment with **1**. To minimize the bias on results, the drug injection and tumor size measurement were conducted by two different persons; the latter was blinded to the identities of the animals. Because paclitaxel comprises 25% weight of **1**, the actual dose of construct is 4 times higher than the indicated value. The 200 mg/kg dose was viscous and represents what is likely an upper limit of concentration. All materials were administered by a bolus injection to the tail vein. Mice were monitored for body weight and behavioral changes. The results are shown in Figure 5.

In comparison with the PBS group, all treatment groups (100s, 100d, 200s, and 200d) showed significantly suppressed tumor growth starting from day 50 ($p < 0.0001$; Figure 5B). The values 100 and 200 reflect the mg of paclitaxel/kg. The "s" and "d" reflect single or double dosings. Among them, the groups treated with double doses of 100 and 200 mg PTX/kg dose levels (100d and 200d) demonstrated better efficacy than the single dose treated groups (100s and 200s) albeit with a lack of statistic significance due to the small sample size (Figure 5C). Encouragingly, the tumor growth was completely arrested in the group treated with double doses of 200 mg PTX/kg (200d). Over the 70 day experiment period, three mice perished: one in the group of 200s, and two in the group of 200d (no animal deaths, abnormal weight

(31) Desai, N.; Trieu, V.; Yao, Z.; Louie, L.; Ci, S.; Yang, A.; Tao, C.; De, T.; Beals, B.; Dykes, D.; Noker, P.; Yao, R.; Labao, E.; Hawkins, M.; Soon-Shiong, P. Increased antitumor activity, intratumor paclitaxel concentrations, and endothelial cell transport of cremophor-free, albumin-bound paclitaxel, ABI-007, compared with cremophor-based paclitaxel. *Clin. Cancer Res.* **2006**, *12*, 1317–1324.
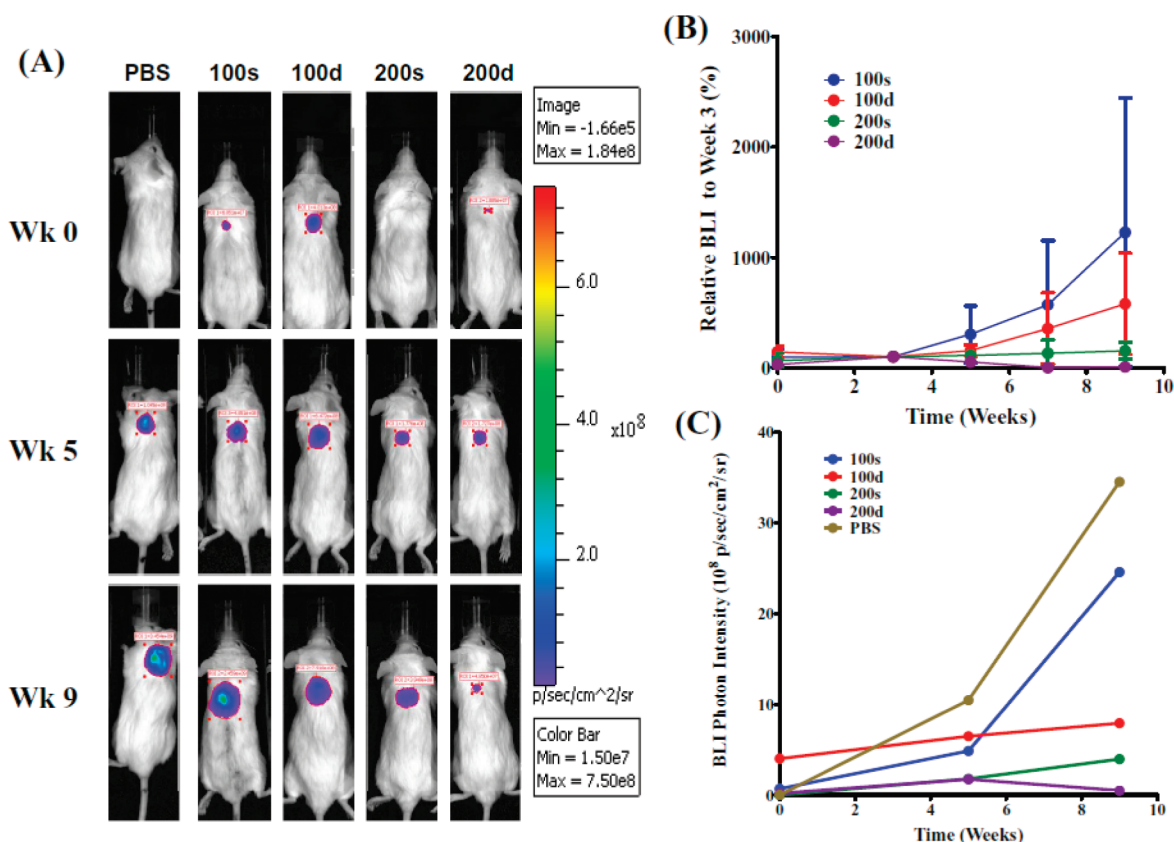
Figure 6. BLI evaluation of the therapeutic efficacy of **1** in SCID mice bearing PC-3-h-luc xenografts. (A) Representative BLI images of four treatment groups and PBS control. The photon intensity of the BLI images is shown on the same scale. (B) Comparative presentation of BLI signals of the four treatment groups. The relative BLI signals at the given week were normalized to the data at week 3 (set at 100%) for all individual mice. (C) Absolute BLI photon intensity quantification of the five tumor-bearing mice shown in (A).

loss or behavioral changes were observed over an extended period when the doses were administered into normal Balb/c mice), suggesting multidose treatment with **1** at <200 mg/kg for future comprehensive evaluations using the same tumor xenograft model.

Given the established role of BLI in the longitudinal monitoring of tumor burden in therapy intervention studies in small animal models,[32] we employed BLI to noninvasively monitor the tumor cell viability during the 10-week treatment experiment period. The results are shown in Figure 6.

Consistent with the caliper measurement (Figure 5), the BLI results shown in Figure 6 clearly demonstrate the tumor growth suppressing effect of **1** in all treatment groups as compared to the control group, while virtually no tumor BLI signal increase was observed in the group of 200d. As shown in Figure 6B, the therapeutic efficacy exhibited by the four dosing plans clearly follows the order of 100s < 100d < 200s < 200d. However owing to the small sample size, the order was not of statistical significance. Compared to the results in Figure 5, the groups of 100d and 200s switched the order

of therapeutic efficacy (Figure 6B,C). This is likely because the caliper reading just provides the physical size of tumor, whereas the BLI photon signal is a direct measure of the tumor cell viability, namely, the luciferase expression in live tumor cells.

By performing Pearson's correlation tests, we found out that the correlation between the tumor size (caliper measures) and tumor cell viability (BLI intensity) was dependent on the treatment dosing plan. As shown in Figure 7, the 100s and 100d groups showed statistically significant correlations where the Pearson r values are 0.775 and 0.754 ($p < 0.0001$), respectively. In the 200d group, the tumor volumes were arrested under 51 mm^3 and the tumor cell viability remained low throughout the study period. The 200s group showed no significant correlation (Pearson $r = 0.130$; $p = 0.4777$) because few tumors in the group reached the size of >200 mm^3. Interestingly, the slopes of linear regressions of 100s, 100d, and 200s are 0.292 ± 0.035, 0.099 ± 0.013, and 0.006 ± 0.009, respectively, indicating that the tumor cell viability was abated by the corresponding treatment plan, which is consistent with the trend of the therapeutic efficacy shown in Figure 6B,C: 100s < 100d < 200s < 200d.

(32) Klerk, C. P.; et al. Validity of bioluminescence measurements for noninvasive in vivo imaging of tumor load in small animals. *Biotechniques* **2007**, *43* (1 Suppl.), 7–13.
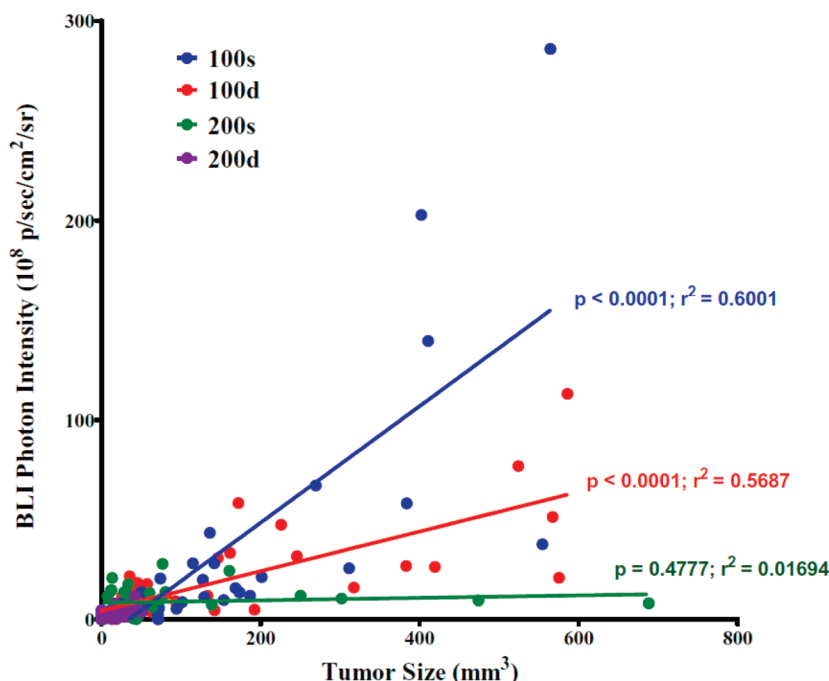
Figure 7. Correlations between the tumor size (caliper measures) and tumor cell viability (BLI photon intensity).

Conclusions

This study suggests that PEGylated triazine dendrimers are biocompatible architectures in acute dosing strategies. The materials are reasonably, yet heterogeneous, due in large part to the distribution of PEGylated dendrimers that are observed. Dendrimer **1** joins a handful of dendrimer architectures that have shown *in vivo* efficacy in cancer models including PAMAM constructs from Baker's laboratory and the polyesters and polylysine dendrimers from Fréchet and Szoka.[13,14] Baker's construct utilizes methotrexate.[12] Fréchet and Szoka have explored camptothecin[13] and doxorubicin.[14] We now add paclitaxel to the list of drugs which have been successfully incorporated into dendrimers that are efficacious *in vivo*. There is clearly room for improvement. In the clinic, Taxol doses at 13.4 mg/kg/day; and Abraxane doses at 30 mg/kg/day or 40 mg/kg every 7 days for three doses.[33] The system could be further improved by increasing tumor uptake by increasing the circulation time in blood and decreasing liver uptake, a process that is probably a result of dendrimer aggregation. Future systems could explore strategies to ameliorate aggregation such as the use of longer PEG chains. However, success is far from guaranteed in this case. As these constructs rely on passive accumulation in the tumor which is likely influenced by size, reducing the propensity for aggregation, and concomitantly the size, could lead to materials that do not passively accumulate and, as a result, are devoid of biological activity. Compared with clinically relevant materials, the actual dose of paclitaxel for **1** in mouse models exceeds that of Abraxane and Taxol formulations by $3-5\times$.[31] Still, there is reason to be optimistic given both the power of physical organic chemistry and the wealth of related paclitaxel-containing macromolecular constructs that are advancing the field.[34–44]

(33) Feng, Z.; Zhao, G.; Yu, L.; Gough, D.; Howell, S. B. Preclinical efficacy studies of a novel nanoparticle-based formulation of paclitaxel that out-performs Abraxane. *Cancer Chemother. Pharmacol.* **2010**, *65*, 923–30.

(34) Albain, K. S.; Belani, C. P.; Bonomi, P.; O'Byrne, K. J.; Schiller, J. H.; Socinski, M. PIONEER: a phase III randomized trial of paclitaxel poliglumex versus paclitaxel inchemotherapy-naive women with advanced-stage non-small-celllung cancer and performance status of 2. *Clin. Lung Cancer* **2006**, *7*, 417–419.

(35) Beeram, M.; Rowinsky, E. K.; Hammond, L. A.; Patnaik, A.; Schwartz, G. H.; de Bono, J. S.; Forero, L.; Forouzesh, B.; Berg, K. E.; Rubin, E. H.; Beers, S.; Killian, A.; Kwiatek, J.; McGuire, J.; Spivey, L.; Takimoto, C. H. A phase I pharmacokinetic(PK) study of PEG-paclitaxel in patients with advanced solid tumors. *Proc. Am. Soc. Clin. Oncol.* **2002**, *21*, 405.

(36) Meerum Terwogt, J. M.; ten Bokkel Huinink, W. W.; Schellens, J. H.; Schot, M.; Mandjes, I. A.; Zurlo, M. G.; Rocchetti, M.; Rosing, H.; Koopman, F. J.; Beijnen, J. H. Phase I clinical and pharmacokinetic study of PNU166945,a novel water-soluble polymer-conjugated prodrug of paclitaxel. *Anticancer Drugs* **2001**, *12*, 315–323.

(37) Khandare, J. J.; Jayant, S.; Singh, A.; Chandna, P.; Wang, Y.; Vorsa, N.; Minko, T. Dendrimer versus linear conjugate: Influence of polymeric architecture on the delivery and anticancer effect of paclitaxel. *Bioconjugate Chem.* **2006**, *17*, 1464–1472.

(38) Gao, Y.; Chen, L.; Gu, W.; Xi, Y.; Lin, L.; Li, Y. Targeted nanoassembly loaded with docetaxel improves intracellular drug delivery and efficacy in murine breast cancer model. *Mol. Pharmaceutics* **2008**, *5*, 1044–1054.

(39) Vrudhula, V. M.; MacMaster, J. F.; Li, Z.; Kerr, D. E.; Senter, P. D. Reductively activated disulfide prodrugs of paclitaxel. *Bioorg. Med. Chem. Lett.* **2002**, *12*, 3591–3594.

Supporting Information Available: This material is available free of charge via the Internet at http://pubs.acs.org.

MP100104X

(40) Majoros, I. J.; Myc, A.; Thomas, T.; Mehta, C. B.; Baker, J. R. PAMAM dendrimer-based multifunctional conjugate for cancer therapy: synthesis, characterization, and functionality. *Biomacromolecules* **2006**, *7*, 572–579.

(41) Papas, S.; Akoumianaki, T.; Kalogios, C.; Hadjiarapolglou, L.; Theodoropoulous, P. A.; Tsikaris, V. Synthesis and antitumor activity of peptide-paclitaxel conjugates. *J. Pept. Sci.* **2007**, *13*, 662–671.

(42) El Alaoui, A.; Saha, N.; Schmidt, F.; Monneret, C.; Florent, J.-C. New Taxol (paclitaxel) prodrugs designed for ADEPT and PMT strategies in cancer chemotherapy. *Bioorg. Med. Chem. Lett.* **2006**, *14*, 5012–5019.

(43) Zou, Y.; Fu, H.; Ghosh, S.; Farquhar, D.; Klostergaard, J. Antitumor activity of hydrophilic paclitaxel copolymer prodrug using locoregional delivery in human orthotopic nonsmall cell lung cancer xenograft models. *Clin. Cancer Res.* **2004**, *10*, 7382–7391.

(44) Guillemard, V.; Saragovi, H. U. Taxane-antibody conjugates afford potent cytotoxicity, enhanced solubility, and tumor target selectivity. *Cancer Res.* **2001**, *61*, 694–699.